

An Investigation on the Effects of Gases in GTA Welding of a Wrought AZ80 Magnesium Alloy

Argon, helium, and nitrogen, some enriched with hydrogen, were investigated for their effects on melting and penetration

BY M. MARYA, G. R. EDWARDS, AND S. LIU

ABSTRACT. Magnesium alloy components are frequently gas tungsten arc welded despite magnesium's high thermal diffusivity. Gases such as argon, helium, and nitrogen — enriched or not with hydrogen — have been investigated to determine if melting, and in particular weld penetration, can be increased. Images of the arcs, voltage readings, dimensions, defects, and microstructure of weld fusion zones have been examined. Due to a greater first ionization potential, helium increased the constant-current voltage and created more melting than argon. With diatomic gases such as nitrogen and hydrogen, voltage and weld dimensions were even further increased. However, hydrogen caused porosity, and nitrogen interacted with magnesium by leaving a nitride deposit at weld surfaces. While consequences of alloying with nitrogen were probably not disadvantageous, hydrogen pores were of greater concern. Both welding parameters and hydrogen concentration in the arc atmosphere were important in controlling porosity. The two-dimensional heat-flow conditions of fully penetrating welds were capable of eliminating porosity and could make welding with hydrogen additions a possibility to consider.

Introduction

The demand for vehicles with improved fuel efficiency has created greater incentives for the engineering of components of aluminum and magnesium. Among other attractive properties, magnesium alloys have two-thirds the density of aluminum alloys, and their strength-to-weight ratios are greater. However, industrial exploitation of magnesium alloys is still restricted, partly due to magnesium's

low formability. To date, magnesium components are mainly cast, but routes are being developed to produce formable magnesium alloy sheets. In the absence of sheet products, welding has been confined to isolated applications (Ref. 1). However, realizing that welding, like forming, would open a whole new range of applications, weldability of magnesium alloys has recently been investigated with a variety of processes, particularly gas tungsten arc welding (GTAW), laser beam welding, and friction stir welding (Refs. 1–5). Of all commercial magnesium alloys, those with aluminum as the primary alloying element are most weldable using any of these three processes (Refs. 2–6). With arc welding processes, lack of weld penetration is generally a limitation of the magnesium alloys. In arc welding with a nonconsumable tungsten electrode (i.e., GTAW), the electric arc is struck by applying a direct current, an alternating current, or a current with other waveforms. For magnesium alloys, alternating current offers a major advantage over the direct current to initiate a weld pool, and this advantage is the cathodic cleaning of the magnesia covering the surfaces (Ref. 6). However, compared to direct current where the electrode is negative and operates as a cathode, alternating current lowers the heat input to the base material and produces shallower welds, especially when argon is selected over helium (Refs. 6–8). Here, the addition of a diatomic gas, like hydrogen (H₂)

or nitrogen (N₂), to a monatomic gas, like argon (Ar) or helium (He), is proposed to increase the melting of magnesium alloys during GTA welding.

While hydrogen and nitrogen have been safely introduced to argon or helium for increasing weld penetration in transition-metal alloys, their use has not been reported for joining magnesium. The magnesium-hydrogen phase diagram (Ref. 9) shows that hydrogen solubility in magnesium decreases by about 25 wt-% when magnesium solidifies at 650°C. This characteristic alone indicates that hydrogen accumulates rapidly at the solid/liquid interface, and if hydrogen partial pressure is sufficient, gaseous bubbles will form. In general, pores appear in welds when the ratio of solubility at the average pool temperature and at the melting temperature (either in the liquid phase or solid phase) is high (Refs. 8–10). The concentration of a gas absorbed by the weld pool depends upon its partial pressure in the arc atmosphere and the temperatures at the weld pool surface. Knowing that surface temperatures of GTA weld pools must approach the material's boiling temperature (1090°C for magnesium) and that pure magnesium solidifies at 650°C, Sievert's law can be applied to estimate the propensity of hydrogen to generate porosity. For liquid magnesium (Ref. 10), Sievert's law can be represented as:

$$[H] = 608 \cdot p^{1/2} e^{\left(-\frac{24,400}{RT}\right)} \quad (1)$$

where [H] is the total volume of hydrogen in the liquid metal in mL/100 g, p is the partial pressure of hydrogen in the arc expressed in atmospheres, R is the universal gas constant (8.31 J·mol⁻¹·K⁻¹), and T is molten metal temperature (in kelvin). Equation 1 predicts that the equilibrium solubilities at 1-atm hydrogen pressure for 1090° and 650°C are 70.6 and 25.3 mL/100 g, respectively, as validated by independent measurements by Fromageau et al.

KEY WORDS

Magnesium
Gas
Arc Physics
Fusion Zone Dimensions
Porosity
Phase Stability

M. MARYA, G. R. EDWARDS, and S. LIU are with the Center for Welding, Joining, and Coatings Research, the G. S. Ansell Department of Metallurgical and Materials Engineering, Colorado School of Mines, Golden, Colo.

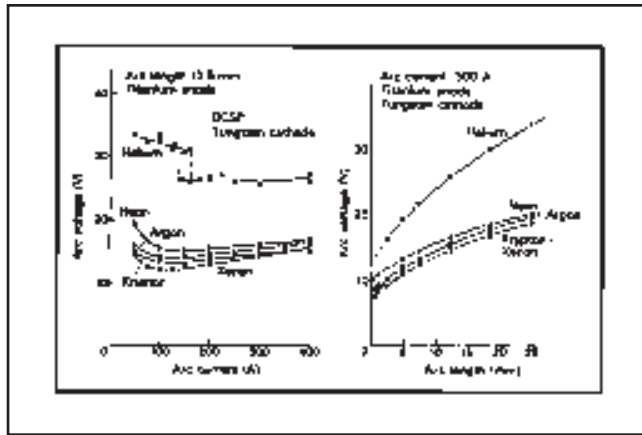


Fig. 1 — Arc voltage with various monatomic gases as a function of arc current and arc length during direct current electrode negative (DCEN) gas tungsten arc (GTA) welding of carbon steel (Ref. 7).

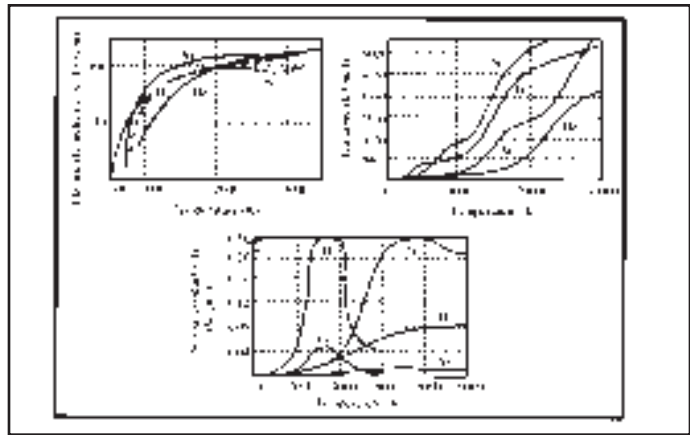


Fig. 2 — Electrical conductivity and enthalpy (Refs. 7, 20), and thermal conductivity of several pure ionized gases as a function of temperature (pressure is one atmosphere) (Refs. 7, 19).

(Ref. 11). It follows that hydrogen solubility in solid magnesium at the melting temperature, being about 25% less, is in the vicinity of 19 mL/100 g. Although all these values of solubility will be affected by welding, the proposed estimates using equilibrium conditions are valuable to assess hydrogen potency in porosity formation. Equation 1 shows that the pressure required to keep all the hydrogen gas in solution is $(70.6/25.3)^2 = 7.8$ atm when the pool cools from 1090° to 650°C. For gas bubbles to form, which requires that the amount of dissolved hydrogen exceeds the equilibrium solubility at 1-atm hydrogen pressure, the hydrogen partial pressure at 1090°C must be greater than $1/7.8 = 0.13$ atm (i.e., hydrogen concentration must exceed 13% of the arc atmosphere). This calculation shows that the minimum concentration of hydrogen to induce porosity is significant in magnesium. A comparable calculation for aluminum would show that hydrogen partial pressure is smaller by about two orders of magnitude (Ref. 8). This prediction that hydrogen potency to produce pores in magnesium is far less than in aluminum has been verified by comparing data from various investigators (Refs. 12, 13). However, no research to date has established if hydrogen is always detrimental to magnesium during welding. Similarly, the effects of nitrogen have not been reported. Further, since the magnesium-nitrogen phase diagram has not been entirely established (Ref. 14), it is even difficult to predict the potential effects of nitrogen on the weld fusion zone. Based upon work of Aizawa et al. on plasma sprays (Ref. 15), an alloying with nitrogen may be expected for the weld region, and this alloying could in fact result in an improved corrosion resistance. However, the literature does not tell how nitrogen will influence the arc and especially how nitro-

gen compares to the other gases under comparable welding conditions.

This research pursues complementary objectives: 1) determine if diatomic gas additions can increase GTA weld penetration in magnesium alloys, 2) determine if hydrogen can be introduced to argon or helium, and 3) investigate the role of nitrogen during arc welding of magnesium. In this paper, the physical properties of gases are first discussed, followed by a description of the experimental procedure and results. The discussion of the results first addresses the effects of gases on the arc, and then their effects on melting, defect formation, and fusion zone microstructure.

Physical Properties of Gases

In GTA welding, the voltage established between the nonconsumable tungsten electrode and the base material is normally self-regulated to deliver a constant current. With the current being approximately invariant, Ohm's law indicates that voltage and electrical conductance of the arc are inversely proportional. The conductance of the arc is a function of its dimensions, particularly the distance between the electrode and the base material (i.e., the arc length), as well as the local values of its electrical conductivity. As a simple definition, the electric arc is a sustained discharged plasma with physical properties that relate mainly to the ionization of its gaseous species. In the arc, electrical conductivity is greater where electrons are generated at low temperatures. A monatomic gas, thus a gas only consisting of unbound atoms in their gaseous state, has a high electrical conductance when its first ionization potential (i.e., the energy barrier to release a first electron) is small. The lower the gas first ionization potential, the smaller is the

voltage necessary to produce a given current, and the smaller are the energy and thus the average arc temperature. Figure 1 (Refs. 7, 16) demonstrates that voltage across a GTA arc decreases noticeably when gases with a small first ionization potential, as found going down the periodic table, are selected. Helium, because of its high first ionization potential (24.6 eV), conducts the current least and consequently requires the greatest voltage of all monatomic gases to carry a given current. Comparatively, arc voltages with argon and particularly xenon are smaller as explained by the smaller first ionization potential of these two monatomic gases (15.6 eV for argon and 12.1 eV for xenon). Since the current carrying capability of the arc depends upon its electron population, itself dependent upon the temperatures established within the arc, any properties that would affect arc temperatures are relevant to GTA welding. Thermal conductivity and specific heat are therefore two important properties that must be considered to understand the effects of the various gases selected for this study.

For monatomic gases, electrical conductivity, heat capacity, and thermal conductivity all increase when first ionization potential decreases (Refs. 7, 16). For diatomic gases, the physical properties are strongly affected by the dissociation that precedes the thermal ionization of the gaseous unbound atoms (Refs. 7, 18–20). The dissociation energy of diatomic nitrogen is greatest (9.8 eV), followed by that of diatomic oxygen (5.1 eV) and diatomic hydrogen (4.5 eV) (Refs. 7, 19). Figure 2 (Refs. 7, 20) compares physical properties of argon, helium, and several diatomic gases. The graph at the top-left corner is a semilog representation of the electrical conductivity as a function of temperature. It is seen that electrical conductivity of

argon is considerably greater than that of helium at temperatures less than about 3000 K. This is a direct consequence of argon's smaller first ionization potential. However, at higher temperatures, the population of charged particles (i.e., positive ions and electrons) rapidly levels off in both gases (Refs. 7, 16) and the electrical conductivities become comparable, at least until secondary ionization takes place. Compared to argon, diatomic nitrogen and diatomic hydrogen exhibit smaller electrical conductivities. Beyond 2000 K, their conductivities are also less than that of helium. Of the properties seen in Fig. 2, enthalpy and thermal conductivity of diatomic gases differ most significantly from those of argon and helium. The top-right corner graph reveals that enthalpies of the diatomic gases are considerably greater than those of argon or helium. As a direct consequence, raising the temperature of these gases will require more energy than with either argon or helium, regardless of the extents of the gas ionization. Diatomic gases also extract thermal energy more efficiently, as well-depicted by the lower graph. The fact that thermal conductivity of hydrogen and oxygen rapidly decrease after 4000 K indicates that a large fraction of the diatomic molecules have already split into single atoms. Due to a substantially greater dissociation energy (9.8 eV), electrical conductivity of nitrogen does not drop before 7000 K. All the property differences depicted in Fig. 2 between argon, helium, nitrogen, and hydrogen will influence GTA welding, particularly the voltage necessary to stabilize the arc, the heat that this arc generates, and thus the heat input to the base material.

Experimental Procedure

To study the effects of monatomic and diatomic gases using a limited number of experiments, only five gases were selected. They were commercially pure argon, argon with 1% and 6% hydrogen, helium with 1% hydrogen, and nitrogen with 1% hydrogen. With the first three gases, the influences of hydrogen additions could be investigated. Further, considering 1% hydrogen, the effects of argon, helium, and nitrogen could be compared. However, a direct comparison of the two diatomic gases, hydrogen and nitrogen, could not be made. In addition to five gases, three currents (30, 40, and 50 A) and four arc lengths (0.5, 1.0, 2.0, and 4.0 mm) were used, leaving a total of 60 bead-on-plate welding experiments and, with two cross sections per weld bead, 120 cross sections to examine.

Bead-on-plate gas tungsten arc (GTA) welding was completed using constant current conditions, a travel speed of 100

mm/min, and a gas flow rate of 40 L/min. A set of 2-mm-diameter tungsten electrodes was prepared with a typical tip angle of 60 deg. When tip wear was observed, the tungsten cathodes were replaced to guarantee consistent and comparable experimental results. A digital multimeter with a precision of 0.01 V and a digital camera with a dark filter were utilized to investigate contributions of the various gases on the arcs. Visual characteristics of the arc as well as voltages, measured at the welding power supply, were captured. This voltage, although not measured directly across the arc, is closely related to the arc voltage, and was therefore sufficient to compare the various gases quantitatively. Later in the paper, this voltage is referred to as welding voltage.

All the welding specimens were fabricated from a single 180-mm-diameter extruded AZ80 magnesium alloy plain cylinder. The selection of a wrought alloy as opposed to a cast alloy guaranteed that the initial material did not contain any pores, in particular hydrogen pores. The AZ80 alloy of this study had approximately 8.50 wt-% aluminum and 0.60 wt-% zinc, as estimated using glow discharge spectroscopy. In this investigation, the extruded cylinder was sliced into 3.8-mm-thick circular plates, which were then ground to exhibit smooth and shiny surfaces. Depending upon welding parameters and gases, partial and fully penetrating welds were obtained. On each plate, six bead-on-plate welds were deposited parallel to each other. No fixtures were applied during welding, as the plates were simply positioned on top of a flat and bulky aluminum support, which also eliminated the need for a secondary root shielding.

After bead-on-plate welding, the specimens were cross-sectioned, ground, and

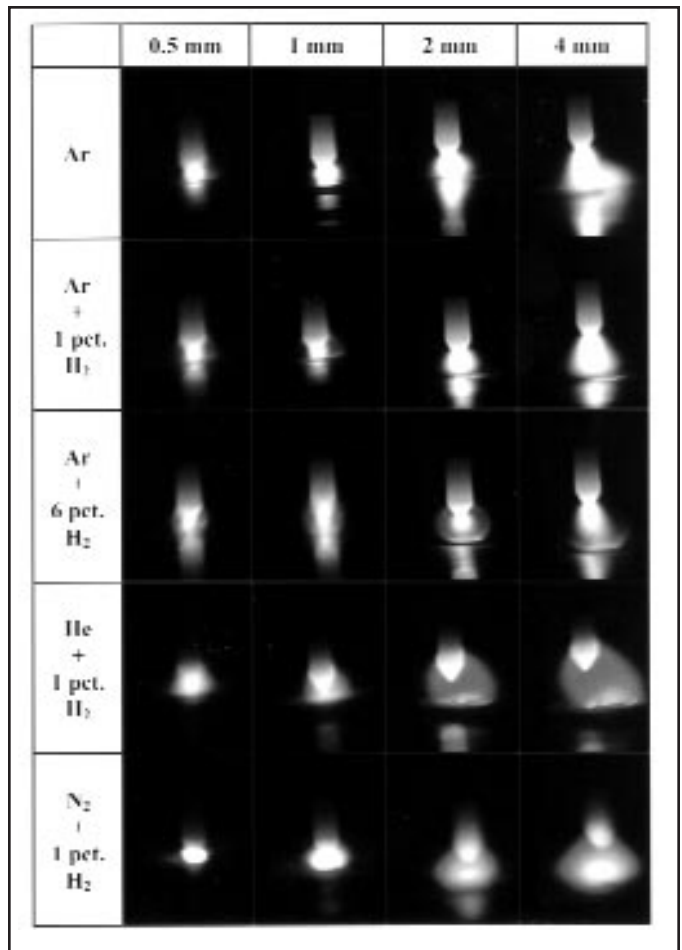


Fig. 3 — Digital images of the arc produced with several combinations of shielding gases and arc lengths (current: 30 A).

polished with silicon-carbide papers and diamond pastes (6 and 1 μm), etched with 2% nital, and examined with a stereomicroscope at magnifications from 10 to 40 \times . Dimensions of fusion zones (penetration and width) were measured and porosity (if encountered) was quantified using conventional image analyses based on area measurements. Optical microscopy, scanning electron microscopy, electron dispersive spectroscopy (EDS), X-ray diffraction (XRD), and thermodynamic calculations were also used to complement the analyses of the weld fusion zones.

Results and Discussion

Arc Morphology

Figure 3 displays digital images of the arc produced using various combinations of gases and arc lengths, as the arcs were viewed from the side. For the purpose of photographing the arc, the welding current of 30 A was preferred. Of the three selected currents, this current generated

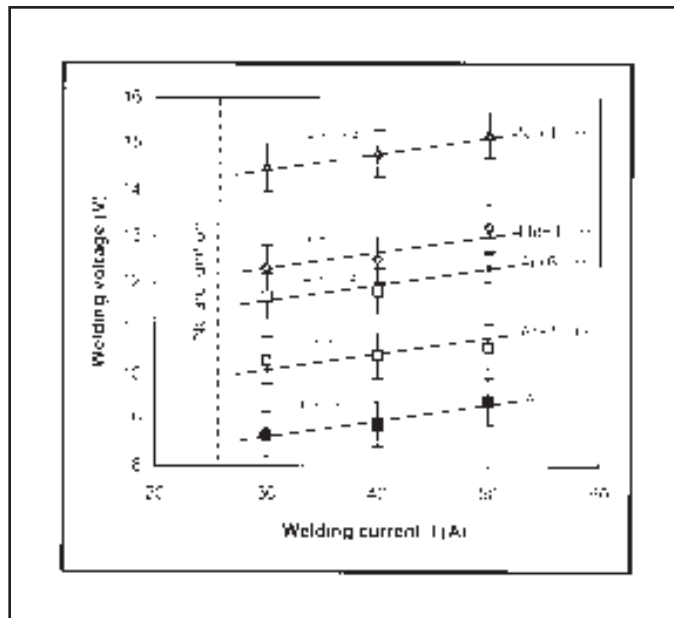


Fig. 4 — Voltage vs. current characteristics for the five gases (arc length: 0.5 mm).

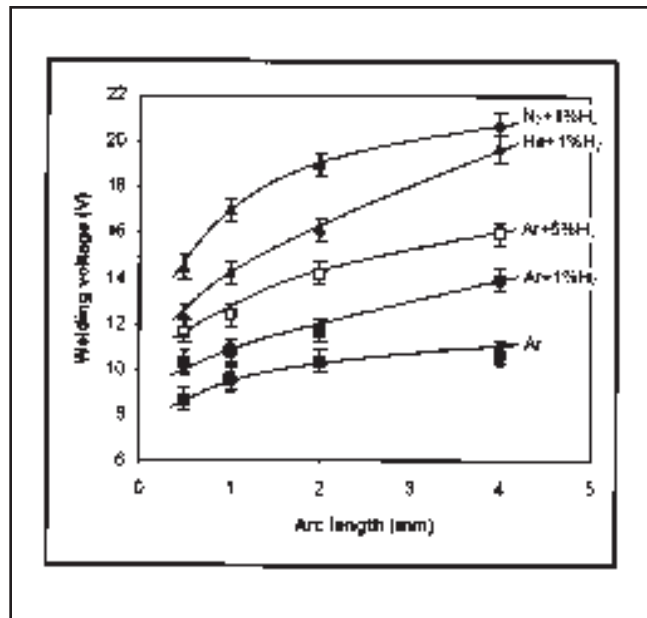


Fig. 5 — Welding voltage vs. arc length for the five selected gases (current: 30 A).

the least heat, and therefore minimized the brightness of the arc on the captured images. With a few exceptions, the images exhibited good contrast and they were clear enough for analyses.

By first examining the images of Fig. 3 from top to bottom, the influence of each gas can be examined. The color of the arc was found to vary with the composition of the gases. Since temperatures, radiation wavelength, and color are related, as proven by emission spectroscopy, the colors captured on the images were important features to examine. Behind the dark filter, the arcs with pure argon were yellow. The additions of hydrogen caused the yellow arcs of argon to become increasingly green. The substitution of argon by helium and nitrogen produced entirely green arcs. The arcs were also considerably larger. A comparison of the various argon arcs reveals that hydrogen did not broaden the arc, as could have been expected from the arc colors observed with helium and nitrogen. On the contrary, the argon-hydrogen arcs appeared as if they were constricted, which was particularly apparent by examining the brightest region of the 2.0- and 4.0-mm arcs. Based upon this observation, the possibility was raised that fusion zone penetration might be improved by the use of hydrogen additions, likely through an increase in current density and thus Lorenz electromagnetic force.

The observation that arcs were narrower in the presence of hydrogen is consistent with Fig. 2, where both thermal

conductivity and specific heat are significantly increased by hydrogen, especially at the low temperatures where hydrogen is still in its diatomic form. In the arc periphery, where temperatures are lower than in the arc central region, hydrogen is therefore most effective in restraining the arc from expanding. In the case of the helium enriched with 1% hydrogen, the arcs did not appear to be as bright as the argon arcs. The arcs were also distinctively deflected in the direction opposite to the displacement of the tungsten electrode. This arc deflection was most evident when the arcs were longer, as seen by comparing the pictures of Fig. 3 from left to right.

Compared to the other gases, the arcs produced with the nitrogen-rich gas were noticeably different. Figure 3 does not indicate that these arcs were deflected. On the contrary, they were quite symmetrical, and therefore the direction of electrode displacement, thus arc deflection, could not be determined, as was found with the other gases. As shown in Fig. 3, the digital images of the arcs with the nitrogen-rich gas were also all blurry irrespective of the welding parameters. These hazy images were attributed to the heavy fumes encountered when welding was conducted with this diatomic gas. Figure 3 shows that the images corresponding to arc lengths of 0.5 and 1.0 mm exhibited the brightest features. This observation could be indicative of exceptionally high arc temperatures, and most probably high welding voltages, since these two characteristics are largely related, as explained previously.

Voltage

Figure 4 shows five voltage-current lines, all constructed from average voltage readings with the different gases and all accompanied with a least-square root equation. The error bars indicate that voltage readings were dispersed within a range that represented about 10% of their values. Due to scatter, the voltage measurements made with the different gases occasionally overlapped. However, the data points could still be properly fit using five distinct straight lines. These five separate lines are proof that electrical conductance (defined as the ratio of current over voltage) for the various arcs differed noticeably. Also, the fact that the five lines were parallel (with a constant slope of 0.04 V/A) indicates that voltage and current varied at a constant rate, and this rate did not depend on the gas.

Regardless of the current, the arcs with pure argon exhibited the smallest voltages, followed by the arcs with argon containing 1% and 6% hydrogen, respectively. On average, the addition of 1% hydrogen increased voltage by about 15% over that of argon, and the addition of 6% hydrogen doubled this voltage increase. The helium enriched with 1% hydrogen increased the voltage even further, leading to an average 25% increase in voltage over the 1% hydrogen-enriched argon gas, and about 40% over the pure argon gas. With nitrogen as a substitute to argon and hydrogen concentration still at 1%, the voltage was increased by 45% beyond that of

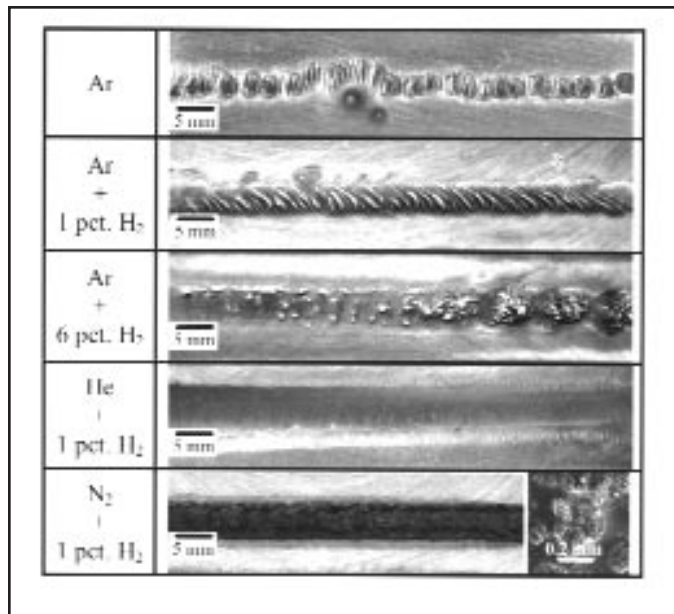


Fig. 6 — Optical macrographs of bead-on-plate welds as seen in top views (current: 30 A, arc length: 4 mm).

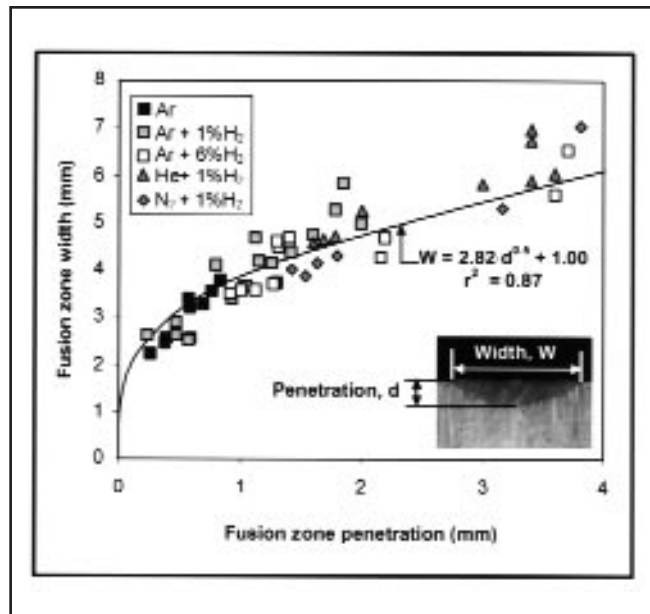


Fig. 7 — Relationship between fusion zone dimensions regardless of gases and welding parameters.

the 1% hydrogen-enriched argon and about 65% over that of the pure argon gas. The dramatic increase in voltage observed with nitrogen compared to argon was well substantiated by Fig. 2, where enthalpy and thermal conductivity of the nitrogen are considerably greater than those of argon and helium. These characteristics suggest that the elevated temperatures needed to ionize and thus create an electrically conductive arc gap require more heat generation with nitrogen. Such a heat generation, and thus heat input to the material, was confirmed by the voltage readings, the fumes observed during welding (which explained the hazy images seen in Fig. 3 with nitrogen), and the bright spots revealed in the same images.

Figure 5 directly complements the set of photographs of Fig. 3 by also describing the effects of both arc length and gas. In agreement with Fig. 3, the voltage (thus the heat generated by the arc) increased with the arc length. As in Fig. 4, the voltage was minimum with argon and increased with the other gases, as given by the sequence shown from top to bottom in Fig. 3. Figure 5 also demonstrates that voltage reached about 21 V when electrode and base material were 4 mm apart, and when 1% hydrogen was added to nitrogen. When examining the effects of arc length, note that voltage appeared to increase at a greater rate in the presence of short arcs.

With both Figs. 4 and 5, the effects of hydrogen could be further analyzed. In both figures, the argon gas containing 1% hydrogen is located about halfway between

the pure argon and the argon with 6% hydrogen. This result indicates that the first 1% hydrogen was about as effective in increasing the voltage as the 5% hydrogen that was subsequently added. Consequently, the arcs produced with hydrogen were conceivably sustained with both a limited dissociation of the diatomic molecules and a slight ionization of the hydrogen atoms. If that is the case, the major contribution of hydrogen would be to cool the arc central region, which would be made possible by increasing thermal conductivity and specific heat of the arc atmosphere.

Weld Fusion Zone Morphology

Figure 6 reproduces optical macrographs of five bead-on-plate welds for which the arcs were presented in the last column of Fig. 3. The welds gathered in Fig. 6 have striking differences. First, starting with the weld made with argon, the presence of transverse striations at its surface as well as frequent lateral deviations suggest that the heat input to the base material was unsteady and insufficient to form a stable and penetrating weld pool. In contrast, the introduction of 1% hydrogen to argon clearly improved arc stability, as the welds were straight and rather indistinguishable from beginning to end. Since the striations at the weld surface were still present, melting also probably occurred within a shallow depth under the surface. However, with an addition of 6% hydrogen, the welds were distinctly wider, as ex-

pected from the voltage measurements presented previously. With 6% hydrogen, spherical-like protrusions, perhaps representing subsurface pores caused by the rejection of hydrogen during solidification, also became visible. When helium was replaced by argon, the widths of the welds were further increased. The surface of the welds was also smooth, a condition that signaled the presence of lesser defects. If that was indeed the case, the 1% hydrogen added to helium could be advantageous. When nitrogen was selected as replacement to argon or helium, weld surface looked noticeably different. As seen in Fig. 6, the coloration of the nitrogen-rich welds was darker. Closer examination by scanning electron microscopy revealed that an agglomerate of fine particles, as shown by the inset image, covered the entire weld surface. Such proof of chemical interactions between the weld fusion zone and nitrogen will be further developed later where the bulk of the fusion zone will be examined in great detail.

Relationships between penetration and width of fusion zones were searched to further characterize the morphology of the produced bead-on-plate welds. As shown in Fig. 7, widths, as seen in Fig. 6, and penetration of the fusion zones were mathematically related irrespective of the gases. Since dimensions of fusion zones were at a first estimate interdependent, the results of Figs. 6 and 7 infer that fusion zone penetration with the hydrogen additions was greater than those made with pure argon, and the same ranking of gases seen for the

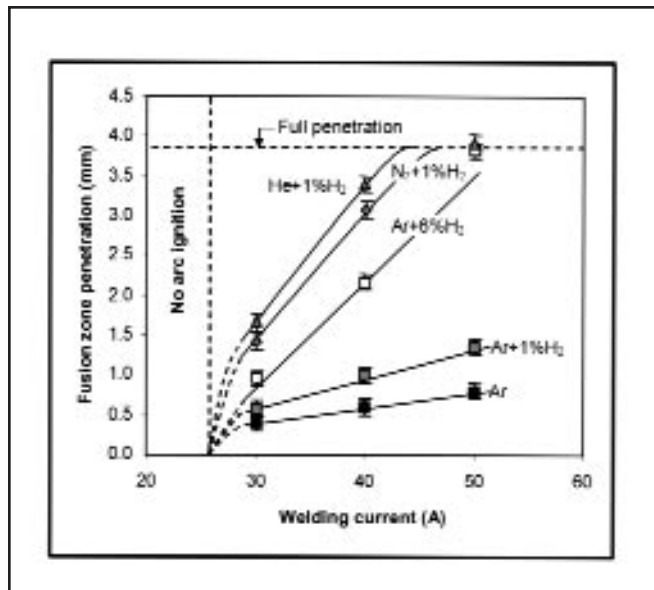


Fig. 8 — Fusion zone penetration vs. welding current for the five gases (arc length: 0.5 mm).

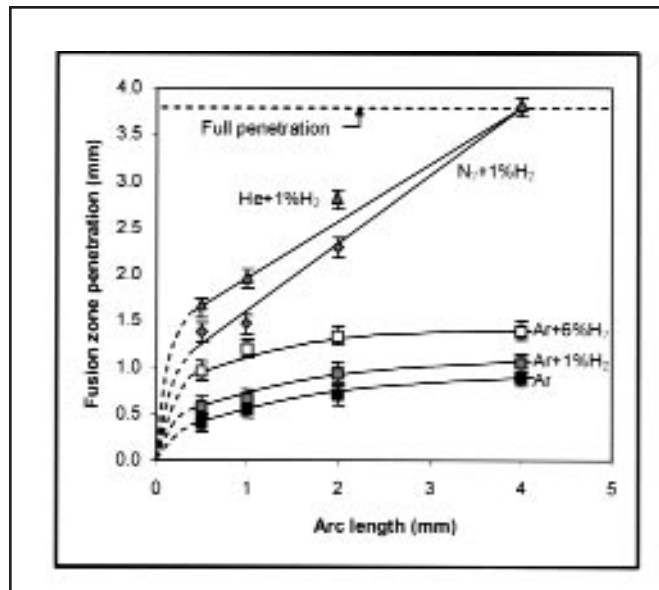


Fig. 9 — Fusion zone penetration vs. arc length for the five gases (current: 30 A).

voltage probably applied to the fusion zone penetration.

Figures 8 and 9 specifically show how fusion zone penetration with the different gases varied as a function of arc length and current. Despite scatter caused by measurements on different cross sections, the scatter was small enough to guarantee excellent comparisons. Both Figs. 8 and 9 appear to substantiate the ranking earlier established with the voltage readings, except that the helium with 1% hydrogen gas produced slightly greater voltages than the 1% enriched nitrogen gas. As found for the voltage, fusion zone penetration increased with both arc length and current. In contrast with voltage readings, however, the slopes for each line seen in Figs. 8 and 9 varied differently from one gas to the other. The argon line exhibited the smallest slope, followed by that of the argon with 1% hydrogen and that of the argon with 6% hydrogen. The lines for the helium and nitrogen gases were noticeably steeper, although precise values for their slopes could not be determined from the two data points only available. Figures 4, 7, and 8, among others, clearly reveal that enlargements of the fusion zones are to some extents related to the voltage readings. Despite significant scatter, Fig. 10 confirms that such a correlation between fusion zone penetration and voltage existed. Figure 10 not only describes the effects of both voltage and current on fusion zone penetration, it also clearly shows that differentiating between gases becomes practically irrelevant when the voltage is considered.

Figures 8–10 also reveal that the fusion zones left by the nitrogen enriched with 1% hydrogen were slightly smaller than those anticipated from the voltage readings — Figs. 4, 5. An explanation can perhaps be found by considering the distinct arc profiles seen in Fig. 3 for the nitrogen-rich gas. With nitrogen as a substitute for argon or helium, both the arcs and the fusion zone penetrations indicate that more heat must have been dissipated into the surrounding of the arc. In other words, nitrogen likely created less energy density than the other gases, although overall heat generated within the arc was greater, as indicated by voltage. This possibility is also strongly suggested by Fig. 2, which indicates that nitrogen had the greatest electrical conductivity of all the gases, in addition to a particularly high enthalpy.

Similar to the effects of nitrogen, the effects of the hydrogen concentration added to argon could also be further examined. As mentioned earlier for the voltage, the line for the 1% hydrogen argon gas was located approximately halfway between the lines of the pure argon and the argon with 6% hydrogen. Figures 8 and 9 indicate that the contribution of 1% hydrogen on the fusion zone dimensions was closer to that of pure argon than to that of the argon with 6% hydrogen. This result, which might appear counterintuitive at first, could also simply suggest that the heat flow had changed, as voltage started to exceed some critical values from which heat flow quickly changed from three-dimensional to two-dimensional (Refs. 6, 22, 23). Fig-

ure 10 confirms that fusion zone penetration and voltage were not proportional to each other, but that fusion zone penetration appeared to increase at a greater rate with the voltage.

Weld-Gas Interactions

The cross-sectional views of Fig. 11 demonstrate that hydrogen is a source of porosity, as theorized previously, whereas nitrogen created weld fusion zones with two distinct regions, which for convenience were designated as FZ1 and FZ2. The first region, FZ1, possessed the normal composition and microstructure of welds made with the monatomic gases, and therefore will not be described in this article. However, the second region found in the upper part of the weld fusion zone, FZ2, revealed an unusual microstructure, as already detected in Fig. 6. In this section, interactions between the AZ80 magnesium alloy and gases like hydrogen and nitrogen are discussed.

Effects of Hydrogen

As suggested in Fig. 6 with the weld produced with 6% hydrogen, Fig. 11 confirms that large spherical pores were encountered when hydrogen was present in the arc atmosphere. However, based upon Figs. 6 and 11, the size and perhaps amount and concentration of pores appeared to be influenced by the concentration of hydrogen, the gas that is mixed with hydrogen, as well as the current that is selected. In this section, the influence of welding parameters is therefore pri-

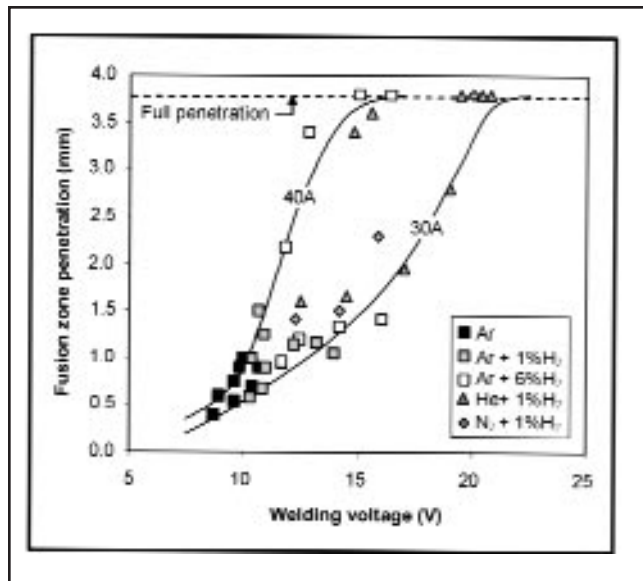


Fig. 10 — Fusion zone penetration vs. welding voltage at two current levels (40 and 50 A), as measured using arc lengths from 0.5 to 4.0 mm

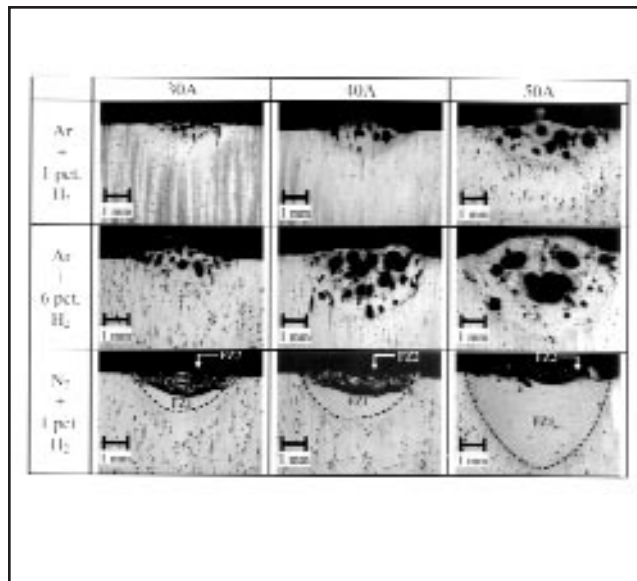


Fig. 11 — Optical micrographs of bead-on-plate welds produced with various combinations of current and gas (arc length: 0.5 mm).

mary to discuss. Since porosity is the result of a nucleation and growth process depending upon mass transport and solubility of hydrogen (Ref. 21), the effects of process parameters that affect hydrogen transport, particularly the arc length and the current, were studied. Further, relations with weld fusion zone morphology, already discussed, were searched.

In Fig. 12, the concentration of hydrogen pores (defined in percent of fusion zone area) at currents of 30 and 40 A is graphically represented as a function of the arc length for each of the hydrogen-enriched gases. Due to variations between weld cross sections, the data were considerably dispersed. While the contribution of current to porosity could not be established using the two currents shown in Fig. 12, a clear correlation between pore concentration, arc length, and hydrogen concentration was found. Figure 12 shows that porosity decreased when the arc length was increased and when hydrogen concentration was reduced.

To understand this last result, some of the results already presented must be reviewed. First, recall that voltage stepped up significantly when the arc length was increased (Fig. 5) and that resulted in wider and deeper weld fusion zones — Figs. 7 and 9. Also, full penetration occurred with a shorter arc when the 1% hydrogen-enriched helium gas was used with a current measuring at least 40 A — Fig. 8. When these conditions were satisfied, porosity was reduced to the greatest extent. In fully penetrating welds, and in welds where fusion zone penetration was over two-thirds of the workpiece thick-

ness (Refs. 22, 23), the heat flow could be categorized as two-dimensional. A consequence of two-dimensional heat flow is that cooling rates are typically one to two orders of magnitude smaller (Refs. 4, 6, 8, 22, 23). Based upon Fig. 12, in welds associated to two-dimensional heat flows, the hydrogen dissolved in liquid magnesium had sufficient time to diffuse out of the pool and effectively reduce porosity. The concentration of pores was considerably different when the arc length was reduced. The fusion zone then partially penetrated into the base material (Fig. 9) and established three-dimensional heat flow conditions, where cooling is comparatively faster.

To address the mechanisms of pore formation, pore diameters were measured, and pore size distributions were established for various welding parameters and the 6% hydrogen gas. Figure 13 shows that the nucleation and growth of pores within the liquid pool did not appear to be measurably restricted by the faster cooling of partially penetrating welds. In fact, Fig. 13 shows that the shallow fusion zones produced with the 0.5-mm arcs and the current of 30 A, where heat flow was three-dimensional, included more pores of any sizes than any other welds considered in Fig. 13. In contrast, population and size of pores were considerably less when the heat flow was two-dimensional, as promoted by the 4-mm arc length. Regardless of welding parameters, Fig. 13 reveals that the population in any given pores gradually decreases as their average diameter increases. This trend demonstrates that

there was always sufficient hydrogen to nucleate small hydrogen pores regardless of the welding parameters. With both large currents and extended arc lengths (i.e., two-dimensional heat flow conditions), the larger pores were eliminated. Porosity was practically eliminated, not because nucleation and growth of pores were restricted, but because hydrogen could leave the weld pool.

Effects of Nitrogen

Figure 14A–D depicts optical and secondary electron images with EDS and XRD results for the region in Fig. 11 that has been designated as FZ2. This new region demonstrates that a measurable amount of nitrogen had permanently entered the weld, most particularly its upper part, FZ2. In one of two reasonable explanations, nitrogen interacted with the weld pool well before its dimensions reached that of the fusion zone. The presence of nitrogen at the weld pool surface, either in solution or as a nitride layer covering the pool, could explain why hydrogen did not induce porosity. In this situation, the contribution of nitrogen would have been to prevent hydrogen to enter the weld pool. Alternatively, nitrogen could have been dissolved in the entire fusion zone, implying that during solidification, hydrogen would have been gradually rejected by the fast-growing magnesium solid phase. In this second explanation, FZ2 would have formed the last, after the material in FZ1 would have solidified without being effectively influenced by hydrogen or nitrogen. To vali-

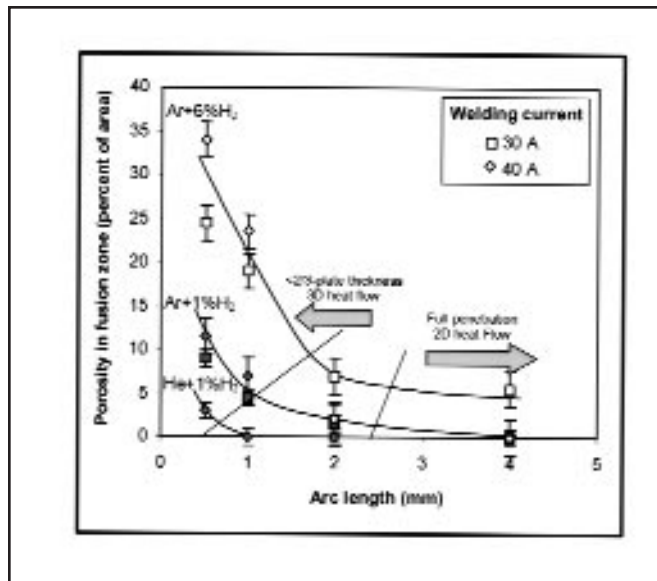
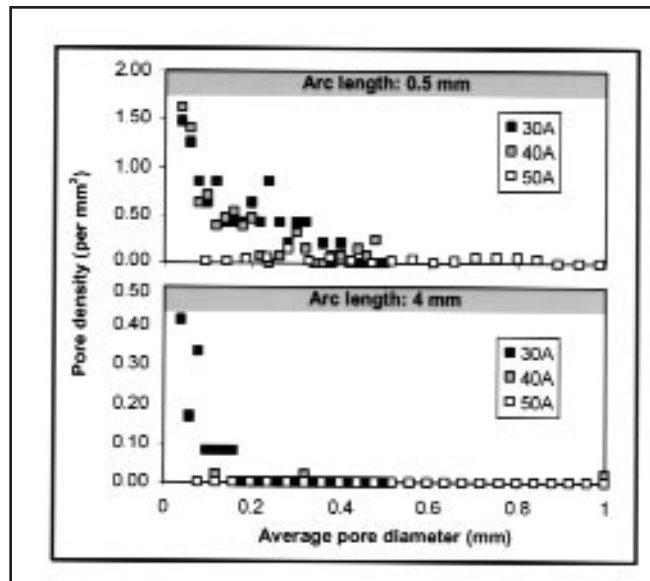


Fig. 12 — Porosity vs. arc length for the hydrogen-containing gases (current: 30 A).



13 — Pore size distribution as a function of arc length and current for the welds produced with the 6% hydrogen-enriched argon gas.

date this second explanation, hydrogen would have been dissolved in restricted amounts in the magnesium liquid phase. Reduced hydrogen solubility, thus low hydrogen partial pressure for pore nucleation, could well explain the absence of pores in all the fusion zones made with nitrogen. Although a complete understanding of the interaction between the magnesium weld pool, nitrogen, and hydrogen might be out of reach given the initial purposes of this study, the data of Fig. 14 are worth examining to better understand weld formation with the nitrogen-rich gas.

Figure 14A and B clearly shows that FZ2 exhibited an uncharacteristic banded microstructure. Such microstructure is as intriguing and puzzling as the presence of the two regions, FZ1 and FZ2. The banded microstructure of FZ2 indicates that nitrogen had entered the weld pool, and had possibly partitioned from a magnesium-rich phase to periodically reach concentrations large enough to stabilize at least one new nitrogen-rich phase. If that is the case, the rejection of nitrogen from a magnesium-rich phase would demonstrate that this magnesium alloy has no solubility for nitrogen. Thermodynamically, this would mean that enthalpy of mixing for a solution comprising magnesium, its alloying elements, and nitrogen is strongly positive, at least when the solution composition is far from that of the new nitrogen-rich phase. If the microstructures of Fig. 14A and B are the result of normal partitioning, the new nitrogen-rich phase must have formed after the magnesium-rich phase, as would be

seen in a eutectic transformation. In the presence of a eutectic transformation, the temperatures where the alloyed region, FZ2, would be liquid would be lower than that of the AZ80 alloy (i.e., the material of FZ1). The presence of a lower melting point eutectic mixture, although not validated by other measurements or a complete binary phase diagram (unavailable), is in agreement with the observation that FZ2 is located near the weld upper surface, where it would be expected if it had solidified at last.

However, the fact that nitrogen accumulated along concentric bands, well following the solid/liquid interface, also appears to be untypical of eutectic decompositions, and this last explanation may therefore be invalid. Although no data are provided to support this discussion, the unusual phase morphology seen in Fig. 14A and B may be better explained if capillarity is considered. Rejection of nitrogen from magnesium-rich growing dendrites and transport of nitrogen along the dendrite boundary toward the dendrite tips (driven by capillarity) would be a satisfactory explanation for the banded microstructures of Fig. 14A and B, if supporting data were available. In that particular situation, nitrogen would constantly advance at the same time as the solid/liquid interface until the nitrogen buildup would become enough for a new phase to form and magnesium to continue solidifying beyond the magnesium nitride phase.

Figure 14C presents a typical energy dispersive spectrum for the darker phase seen in the banded microstructure of Fig.

14A and B. The inset secondary electron image, accompanying the energy spectrum, reveals that this new phase is less conductive than magnesium (because brighter in the SEM), and also hard and brittle, as revealed by its granular appearance. The EDS measurements revealed that nitrogen constituted 40 at.-% of this brittle-looking phase, whereas nitrogen was not present in the magnesium-rich phase, as was suspected from previous analysis. These measurements not only confirm that magnesium and nitrogen did not mix, but that nitrogen and magnesium formed a stoichiometric compound with 40 at.-% nitrogen. Measurements by XRD, presented in Fig. 14D, identified this phase as the normal magnesium nitride phase, Mg₃N₂. Compared to other nitrides, magnesium nitride could have been expected. Of the elements present in an AZ80 alloy (i.e., magnesium, aluminum, and zinc), magnesium's interaction with nitrogen is the strongest, as indicated by comparing Pauling's electronegativity differences with nitrogen, or comparing free energies of magnesium nitride, aluminum nitride, and zinc nitride.

To determine when during welding nitrogen interacted with magnesium, thermodynamic calculations of the equilibrium state of an equi-molar mixture of magnesium, nitrogen, and hydrogen were conducted. Although the proposed stoichiometry is likely different from those found in the weld, results of this calculation were sufficient to incorporate temperature in the analysis. Results of the thermodynamic calculation are graphi-

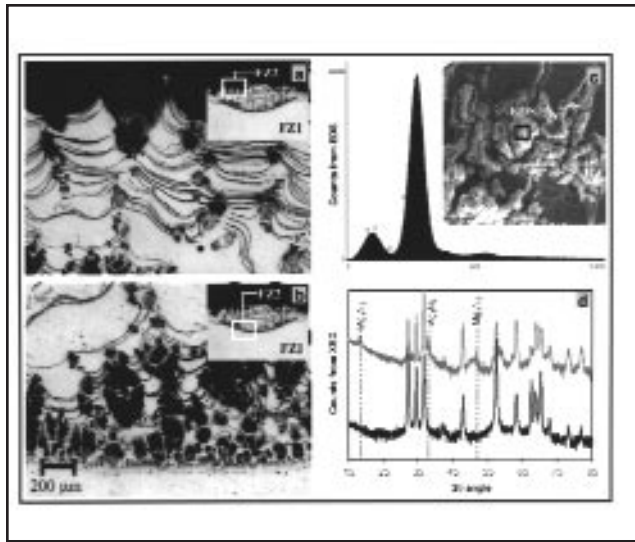


Fig. 14 — Microstructures of the FZ2 region shown in Fig. 11. A and B — Optical micrographs; C — secondary electron image with an EDS spectrum; D — X-ray diffracted intensities of the surface of a weld made with nitrogen enriched with 1% diatomic hydrogen gas.

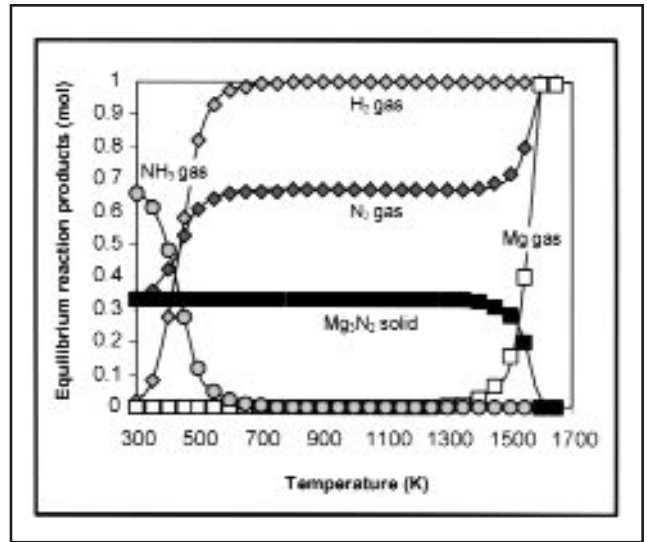


Fig. 15 — Equilibrium products of the equi-molar reaction between magnesium, hydrogen, and nitrogen as a function of temperature..

cally represented as a function of temperature in Fig. 15. In this figure, it is confirmed that the magnesium nitride phase, Mg_3N_2 , was the most stable equilibrium product. However, it is also shown that the Mg_3N_2 phase formed at much higher temperatures than anticipated (about 1500 K), and certainly at temperatures where magnesium was still in a gaseous state. This new result therefore strongly indicates that some unknown fraction of the magnesium nitride seen in Fig. 14 had formed in the arc atmosphere before condensing on top of the weld. Consequently, the first analysis, suggesting that hydrogen was prevented from entering the weld pool because of nitrogen at the weld surface, is validated. This new result still does not mean that the second explanation, invoking the nitrogen partitioning, is invalid. It simply means that understanding weld pool formation in the presence of nitrogen is more complicated than initially thought and requires further research.

Conclusions

The effects of gases, in particular hydrogen and nitrogen, have been investigated with the general objective of increasing melting during GTA welding of magnesium alloys. The following conclusions were reached:

- The weld fusion zone dimensions, particularly the penetration (Fig. 7), were increased with gases having a high first ionization potential, because voltage and thus heat input (under a constant current condition) were increased — Figs. 4, 5.

Helium, due to its high first ionization potential (24.5 eV), produced deeper fusion zones than argon (15.9 eV).

- When 1% hydrogen was added to either argon or helium, the fusion zones were more penetrating than with only the monatomic gases. Also, nitrogen substituted for either argon or helium, generated even more melting, although its first ionization potential is less than that of either argon or helium. The properties of diatomic gases (Fig. 2), particularly enthalpy and thermal conductivity, could well explain the increased voltage and penetration observed with these gases — Figs. 4, 5.

- Despite desirable increase in melting, hydrogen was also a powerful source of porosity — Fig. 13. However, porosity could be prevented by establishing fully penetrating welds, where heat flow is two-dimensional. Due to a slower cooling than in partial-penetration welds, pores could nucleate, grow, and leave the weld pool.

- Regardless of the welding parameters, nitrogen stabilized a second phase near the weld surface — Fig. 14. Although examined in this paper, the interaction between magnesium and nitrogen is not yet well understood.

- Minor additions of hydrogen to argon or helium could be recommended to increase melting. With nitrogen, the properties of the nitride layer must be further investigated.

Acknowledgments

The authors acknowledge Visteon Au-

tomotive Systems (Dearborn, Mich.) for the funding to support graduate-level magnesium welding studies. Because part of this work was achieved at CSM as an undergraduate welding project, the authors acknowledge the technical support of the 2002 welding metallurgy class.

References

1. Friedrich, H., and Schumann, S. 2000. The second age of magnesium — research strategies to bring the automotive industry's vision to reality. *Proceedings of the Second Israeli International Conference on Magnesium Science and Technology*, Beer Sheva, Israel: Magnesium Research Institute, pp. 9–18.
2. Stern, A., and Munitz, A. 1999. Partially melted zone microstructural characterization from gas tungsten-arc bead-on-plate welds of magnesium AZ91 alloy. *Journal of Material Science Letters* 18: 853–855.
3. Weisheit, A., Galun, R., and Mordike, B. L. 1998. CO₂ laser beam welding of magnesium-based alloys. *Welding Journal* 77 (4): 149-s to 154-s.
4. Marya, M., Edwards, G. R., Marya, S. K., and Olson, D. L. 2001. Fundamentals in the fusion welding of magnesium and its alloys. *Proceedings of Seventh International Symposium of the Japan Welding Society on Today and Tomorrow in the Science and Technology of Welding and Joining*, Ed. T. Ohji. Tokyo, Japan: Japan Welding Society.
5. Zhao, H., and DebRoy, T. 2001. Pore formation during laser beam welding of die-cast magnesium alloy AM60B — mechanism and remedy. *Welding Journal* 80(8): 204-s to 210-s.
6. *ASM Handbook*, Vol. 6, *Welding*,

Brazing and Soldering. 1993. Materials Park, Ohio: ASM International.

7. Lancaster, J. F. 1984. *The Physics of Welding*, Second Edition. U.K.: Pergamon Press.

8. Lancaster, J. F., 1999. *Metallurgy of Welding*, Sixth Edition: Abington, Cambridge, U.K.

9. Baker, H., and Okamoto, H. 1992. *ASM Handbook*, Vol. 3, *Alloy Phase Diagrams*. Materials Park, Ohio: ASM International.

10. Popovic, Z. D., and Piercy, G. R. 1975. Measurement of the solubility of hydrogen in solid magnesium. *Metallurgical Transactions* 6A(10): 1915-1917.

11. Fromageau, R., Mairy, C., and Tzanétakis, P. 1980. Hydrogen dissolution in magnesium: a resistometric study under pressure. *Scripta Metallurgica* 14: 395-398.

12. Saperstein, Z. P., Prescott, G. R., and Monroe, E. W. 1964. Porosity in aluminum welds. *Welding Journal* 40(10): 443-s to 453-s.

13. Woods, R. A., 1974. Porosity and hydrogen absorption in aluminum welds. *Welding Journal* 53(3): 97-s to 108-s.

14. Wriedt, H. A. 1988. *Mg-N (Magnesium-Nitrogen), Phase Diagrams of Binary Magnesium Alloys*. Metals Park, Ohio: ASM International, pp. 205-208.

15. Aizawa, T., Kuwahara, H., and Luangvaranunt, T. 2000. Surface modification of magnesium base alloys by gas/plasma nitridation. *Proceedings of Magnesium Alloys 2000*, Nagaoka City, Japan.

16. Jackson, C. E. 1960. The science of arc welding. *Welding Journal* 39: 129-s to 140-s, 177-s to 190-s, 225-s to 230-s.

17. Milner, D. R., Salter, G. R., and Wilkinson, J. B. 1960. Arc characteristics and their significance in welding. *British Welding Journal* 2: 73-88.

18. Onsoien, M., Pieters, R., Olson, D. L., and Liu, S. 1995. Effect of hydrogen in an argon GTAW shielding gas: arc characteristics and bead morphology. *Welding*

Journal 74(01): 10-s to 15-s.

19. Allim, C. J. 1986. Nitrogen absorption from welding arcs, IIW Doc. 212-569-86: International Institute of Welding.

20. Tusek, J., and Suban, M. 1998. Influence of hydrogen in argon as a shielding gas in arc welding of high-alloy stainless steels, IIW Doc. 212-938-98: International Institute of Welding.

21. Devletian, J. H., and Wood, W. E. 1983. Factors affecting porosity in aluminum welds — a review. *Welding Research Council Bulletin* 290: 1-17.

22. Jhaveri, Moffat, W. G., and Adams, C. 1962. The effect of plate thickness and radiation on heat flow in welding and cutting. *Welding Journal* 41(2): 12-s to 16-s.

23. Burgardt, P., and Heiple, C. R. 1993. Weld penetration sensitivity to welding variables when near full joint penetration. *Welding Journal* 72(9): 341-s to 347-s.

24. www.matweb.com

Call for Papers

The American Welding Society announces a Call for Papers for the 2005 Professional Program to be held as part of Welding Show 2005 on April 26-28, 2005, in Dallas, Texas.

Submissions should fall in one of the following three categories and will be accepted only in a specific format. Individuals interested in participating should contact Dorcas Troche, Manager, Conferences & Seminars via email at dorcas@aws.org for specific details. Deadline for submission of paper is Friday, July 30, 2004.

Technical/Research Oriented

- New science or research
- Selection based on technical merit
- Emphasis is on previously unpublished work in science or engineering relevant to welding, joining and allied processes.
- Preference will be given to submittals with clearly communicated benefit to the welding industry

Applied Technology

- New or unique applications
- Selection based on technical merit
- Emphasis is on previously unpublished work that applies known principles of joining science or engineering in unique ways
- Preference will be given to submittals with clearly communicated benefit to the welding industry.

Education

- Welding education at all levels
- Emphasis is on education/training methods and their successes
- Papers should address overall relevance to the welding industry